



## Using the Remote Sensing Method to Simulate the Land Change in the Year 2030

Burcu Çevik Değerli<sup>1,a,\*</sup> Mehmet Çetin<sup>2,b</sup>

<sup>1</sup>Department of Landscape Architecture, Institute of Science, Kastamonu University, 37200 Kastamonu, Türkiye

<sup>2</sup>Department of City and Regional Planning, Faculty of Architecture, Ondokuz Mayıs University, 55200 Samsun, Türkiye

\*Corresponding author

### ARTICLE INFO

Research Article

Received : 03/10/2022  
Accepted : 01/12/2022

Keywords:

Remote Sensing  
GIS  
LU/LC  
Machine Learning  
MLP-ANN

### ABSTRACT

This study is based with the support of RS-GIS technology on the land use of Samsun Center, as well as the coastal districts of İlkadım, Atakum, Bafra Plain, through the processing and interpretation of satellite images in the summer months of 2000, 2010, 2020. Spatial and temporal variability properties of LU/LC were determined using MLC algorithm, controlled classification approach. The predictive values of the LU/LC change that will occur in 2030, calculated with the MLP-ANN model based on Machine Learning algorithms and mapped with the QGIS 3.16 program. To determine the accuracy coefficient of the model, 2020 LU/LC simulation performed using the transition potential matrix of 2000 and 2010 LU/LC data. The results of simulation were compared the data of land use land cover with the 2020 to evaluate the accuracy of the simulation model. The model of MLP-ANN provided an accuracy of 72% based on the kappa fit index. According to MLP-ANN model 2030 results were an increase of 73.33 km<sup>2</sup> in built up areas, an increase of 56.89 km<sup>2</sup> in bare areas, and a decrease of 129.66 km<sup>2</sup> in green areas. It provided a reference basis for future Samsun urban to rural coastline LU planning and management and LU structure optimization.

[burcu.degerli@omu.edu.tr](mailto:burcu.degerli@omu.edu.tr)

<https://orcid.org/0000-0001-5152-6406>

[mehmet.cetin@omu.edu.tr](mailto:mehmet.cetin@omu.edu.tr)

<https://orcid.org/0000-0002-8992-0289>



This work is licensed under Creative Commons Attribution 4.0 International License

## Introduction

Land Use and Cover (LULC) change of the detection and forecast is an important factor for guiding planning, land resource, sustainable development management. Considering the phenological effect and seasonal adaptation, the estimation and detection of the same seasons for different years from LULC maps will greatly benefit (Lu, Wu, Ma, and Li, 2019). Land use has been taking place in line with the possibilities offered by the land cover since the existence of human beings (Saleem et al. 2018).

An urban area is a mosaic of different landscape features or land use (e.g., impermeable surfaces, green areas, residential areas, planting areas, etc.) and has different thermal properties (Wu, 2014; Zhou, Pickett, & Cadenasso, 2017). With the increase in urbanization, land use is developing negatively. Farmland, wetlands and forests are demolished and forests are converted into farmland (Blanco-Canqui and Lal, 2008). Nowadays, the integration of surfaces of impermeable, which is a product

of increasing construction and the surfaces of paved, and decreasing forests and agricultural lands have caused the problems of environment such as landslides, floods environmental pollution, and in cities (Fernando, Dimitrova, and Sentic, 2012). The change of the soil, which contains water resources and plant existence, also causes the deterioration of the vital cycles that occur with the soil. There is a delicate balance between natural resources and ecosystems. Incorrect land use, which causes the deterioration of the ecological balance, becomes one of the causes of climate change.

Since the 21st century, many studies show that land use change causes natural disasters, energy shortages, food shortages, economic crisis and other social and ecological problems (Yao et al., 2021). Therefore, the IGBP means of international geosphere biosphere program and the IHDP means of global environmental change program suggest research on land use driving force and land change analysis as the main research direction to reduce the negative

impact of the human factor on land (Turner et al., 1995). LULC maps need to be prepared to detect and prevent the rapid industrialization and urbanization of a region, excessive and uncontrolled use of the landscape, and damage beyond the limits of sustainable development. Determining Land Use and Land Cover Changes with Geographic Information Systems and Remote Sensing is a sustainable and economical method that helps planners (Güler, et al., 2007).

The aim of this research is to (i) understand the growth of urban model and its direction, (ii) identify the land use-cover changes by determining the possible future growth scenario through simulations in Samsun, one of the most vulnerable and rapidly growing cities of Turkey. The findings obtained from this study are intended to be useful to regional planners by predicting land use in advance in planning the resident and abundant resources of nature in the region by the enhancing demands in the future.

There are studies on land classification using the Remote Sensing method for Samsun. Güler, Yomralıoğlu, and Reis, (2007) made a land classification using Landsat images of the years 1980-1987-1999 in the area stretching from Samsun Bafra plain to Çarşamba plain. Bağcı and Bahadır, (2019) processed the LULC change in the Bafra Kızılırmak delta with the satellite images of 1987, 2002, 2010 and 2018 using controlled classification technique. Sesli, (2010) examined the changes in the coastline using aerial data images in Samsun in 1935, 1972 and 2006 on the eastern shores of the Black Sea in Turkey. According to the study, the 7 km coastline between Samsun Mert River and Kurtün River was filled more than 95.32 ha along the coastal area between 1935 and 1972 and more than 70.74 ha along the coastal area between 1972 and 2006. Ozturk, (2015) determined the study area in Samsun Atakum center and used the models of MLP-MC and CA-MC in the growth simulation of the district.

When we look at international indexes Ullah et al., (2019), LULC changes were estimated for the period 2032 and 2047 using the matrix of transition potential and the model of CA-ANN estimation obtained from the years data of 2002 and 2017. the CA-ANN model of The accuracy of has been achieved at 72% using the validation modules in QGIS. Lu, Wu, Ma, and Li, (2019) used Landsat satellite images from the summer months of the last 30 years in their study. Cellular Automata–Markov model was used as the estimation algorithm. Alqadhi et al., (2021) used the Multilayer perceptron-neural network (MLP-NN) algorithm to simulate the terrain change. He found the accuracy of the prediction model to be 88%. MohanRajan and Loganathan, (2021) using two hybrid algorithms for land cover change prediction, the compare with MC–LR–CA between MC–ANN–CA made them.

Looking at the literature review, many UA researchers have applied data mining models and different machine learning to predict future the independent UA data and LULC change using dependent. GIS commonly used the models of forecasting are as follows: SLEUTH (slope, land use, exclusion, urban extent, transportation, and hill shade), state and transition simulation model (STSM); land transformation model (LTM); CLUE (conversion of land use and its effects), ANN (artificial neural network cellular automata (CA), Markov chain (MC), land change models (LCM), logistic regression (LR), spatially explicit

landscape event simulation (SELES), and GIS-based weights of evidence (WoE) approach. LU/ LC change for especially aim of predicting for the future was to provide to get useful information to the decision-makers, planning amangement, government officials, and land resource planners, and for taking an effective plan for planning and management in protecting the environment of LU/LC (Bounouh et al 2017; Yirsaw et al 2017; Aburas et al., 2019).

This study was evaluated in terms of (i) site selection being on both urban and rural scales in the direction of increasing urbanization, (ii) being based on current data sets (iii) including simulation as well as change analysis (iii) the program used (QGIS) and the algorithm used (MLP-ANN) differs from other studies.

## Material and Method

Samsun province is coordinate of the 40° 50'- 41° 51' N, 34° 25' and 37° 08' E. It has an area of approximately 9.725 km<sup>2</sup> and consists of 17 districts (Anonymous, Accessed on 05.06.2021). According to TUIK 2020 data, the population of Samsun is 1,356,079. Samsun is the 16th largest province of Turkey in terms of population, and it constitutes 17% of the population of the Black Sea Region and 1.6% of the population of Turkey (Anonymous, Retrieved 02.05.2021). It is located in the coastline of middle part of the Black Sea, between the deltas where the rivers of Kızılırmak and Yeşilirmak flow into the Black Sea. Neighbors of the province, in the north of which the Black Sea is located; Sinop in the west, Tokat and Amasya in the south, Ordu in the east, and Çorum in the southwest. Samsun shows three different features in terms of landforms. The first part is the mountainous part in the south; the part of second region is the plateaus between the mountainous part and the coastline, the third; coastal plains between the highlands and the Black Sea (Municipality, Retrieved 27.01.2022).

Samsun has undergone radical changes in the last 50 years as a result of the settlement pressure concentrated on the coastal areas due to urbanization, population growth and socio-economic developments (Anonymous, Accessed: 06.06.2021). After 1998, the urban settlement area in Samsun increased by 96.32% and grew to approximately 32 km<sup>2</sup>, and this growth generally developed towards agricultural areas. Since 1998, Atakum district has become a second city center (Ozturk, 2017). Atakum has the highest population growth in Samsun Province. (Municipality, 2014). The population of the district was 107,953 in 2008 and 158.031 in 2014 (Anonymous, Retrieved 02.05.2021). The average annual growth rate of the district is around 63.5%, and there is a significant immigrant population from other districts and other provinces in Samsun. The district consists of four structures of morphologic: sloping lands, coastal plains, mountainous areas and low plateaus. The plains of coastal are fertile soils formed by the alluviums of the Kızılırmak River in the west and the Kurtun Stream in the east, but almost all of the plains of coastal have been used for settlement. Intense settlements are also observed in the sloping areas between the low plateaus and the plains of coastal (District Government 2013).

As the study area selection criteria, the population of Atakum district is 202,618 according to 2018 data; the population of the region of İlkadim is 332,230, the population of the region of Canik is 97,564. It is seen that the population in the research area increased in the 28-year period between 1990 and 2018, but the increase occurred more in the western direction, which is called Atakum, unlike the 30-year period between 1960 and 1990. When we look at the 2020 TUIK data, the 3rd crowded district of Samsun has been Bafra District, which is located in the western countryside (Figure 1 and Table 1).

The satellite used in the research are Landsat 8 OLI/TIRS (Collection 2, Level 2), Landsat 7 ETM+ (Collection 1, level 1), satellite data belonging to the summer months of 2000, 2010, 2020 (Table 2). Surface reflection, LEDAPS and LaSRC surface reflectance algorithms found in Landsat Collection 2, Level 2, demonstrate the temporal, spatial and scattering of spectrally varying and absorption effects of water vapor necessary aerosols and atmospheric gases, to reliably characterize the land surface of Earth's automatically corrects (USGS, Retrieved 09.04.2020). a Scan Line Corrector (SLC) on May 31, 2003, error occurred in the Landsat 7 ETM sensor (Enhanced Thematic Mapper) in Landsat 7 ETM+ satellite images, resulting in approximately 22% data loss. Gaps were corrected by applying gap fill to Landsat 7 images of 2010 used in this study with the data accompanying the gap mask file (University, Accessed 01.08.2020). Satellite images and bands used to create LU/LC maps are shown in Table 2. Again, NDVI (Normalized difference vegetation index) maps were created from the same images. Images are selected based on 10% cloud rate. Radiometric and Geometric correction pre-processes were applied. LULC maps were used as the basic input data of the model of MLP-ANN, and NDVI, Dem, Slope, Distance From River (DFR) maps were used as supplementary data for estimation. ArcGIS 10.5, the software used for Image processing and GIS, and SPSS 24 software were used for calculating QGIS 3.16 statistics. The work flow chart of the study is given below (Figure 2).

The detailed process of LULC modeling covers different stages such as data collection, preprocessing, LULC post-classification analysis, validation, classification, LULC change prediction, spatial variables modeling (MohanRajan et al 20020).

In our study, algorithm of MLC was used to classify for images of satellite. The MLC technique was preferred so that it is the efficient and common classification matrix in the literature when the data/locations of correct training are created (Benediktsson, Swain, & Ersoy, 1990; Paola & Schowengerdt, 1995). It uses training sets to estimate the mean values and the variance of the class DN to measure the probabilities and variability of the reflection values (Lee and Song, 2004). However, the accuracy of the classification depends on the reliability and accuracy of the signature set obtained from the RGB band combinations applied image. Signature sets are regions on the image that appear relatively homogeneous, showing each type of LULC, whose homogeneity is confirmed by Google Earth satellite imagery and on-site inspection. The more signature sets are determined, the better results can be obtained.

Descriptive statistics properties (mean values for each spectral band and DN (digital number) variances) are determined with the help of spectral signatures. As described in Congedo, (2016), Spectral signatures are used by Classification Algorithms to label image pixels. Different materials can have similar spectral signatures such as structure and soil (especially when considering multispectral images). If the spectral signatures used for classification are too similar, pixels may be misclassified because the algorithm cannot distinguish these signatures correctly. Therefore, the Spectral Distance of the signatures was evaluated to find similar spectral signatures that should be removed. Spectral signatures collected for the MLC method, however, were checked to be different from each other by measuring the Jeffries-Matusita Distance value, which is very effective for Maximum Likelihood (a value close to 2 indicates different signatures) (Figure 3).

Controlled classification typically involves a series of steps (i) identification of training fields, (ii) spectral signature collection, and (iii) image classification (Alqadhi et al., 2021). The MLC algorithm is implemented in the R programming language in QGIS using the classification of semi-automatic plugin, which developed and created Luca Congedo (Congedo, 2021). The classification algorithm of maximum likelihood is a parametrically controlled classifier. The probability  $D$  of the unknown measurement vector  $X$  is based on the Bayes equation or calculate the weighted distance used to the algorithm (Jamali, 2019).

$$D = \ln(ac) - [0.5 \ln(covc) - [0.5X - Mc]T(covc - 1)(X - Mc)](1)$$

In this study, MLC-controlled classification was performed with the original satellite data bands (LANDSAT) that produced LU/LC maps for 2000, 2010 and 2020. Then, the LU/LC maps were evaluated using the cross-classification method. The LU/LC 2000-2020 variation was observed using classified map features. A table showing the area in square kilometers was created and the area (km<sup>2</sup>) for each LU/LC class and the percentage change in the data set were calculated. accuracy assessment is that the confusion matrix statistically obtained from field data (signature file) and the maps of LU/LC was used for (Jensen, 1986). The accuracy of the LU/LC classes was determined by the kappa statistical coefficient (Table 2).

The classes within the study area were determined as (i) Water (River, Lake, Sea), (ii) Built up (Urban, Roads), (iii) Vegetation (Forest, Cropland, Delta, (iv) Open Land (Bare Soil) (Congedo, 2016).

the future urban LUC of prediction in the determined research area in Samsun, the study includes three main steps: (i) preparation of LULC from satellite images, (ii) preparation of data input for terrain change modeling (iii) modeling of present LULC forecast to calculate future LULC forecast accuracy. Land use and classified images from the years 2000 and 2010 were used to generate a transition potential matrix using the QGIS MOLUSCE tool. NDVI, Distance from river, Dem, Slope were used as additional data for the model. Digital Elevation Model (DEM) which is the map of Elevation made using obtained from the of ALOS PALSAR RTC. The DEM data are extracted for the map of Slope. River networks from DEM data SHP.

Table 1. Research Area District Areas of Populations (Anonymous, Accessed on 02.05.2021)

Administrative units	Area (km <sup>2</sup> )	Population
Ilkadam	155	336.501
Atakum	351	221.082
Bafra	1503	143.443

Table 2. Satellite Images Used in the Study

Satellite	WRS-2 Row/Column	Data History	ID	Bands/Wavelength Spectral range (µm)	Resolution (m)
Landsat 7 ETM+	175/31	31.07.2000	LE07-L1TP-175031	Band 1/ 0.450 -0.515 Blue	30
				Band 2/ 0.525 -0.605 Green	30
				Band 3/ 0.630 -0.690 Red	30
				Band 4/ 0.750 -0.900 Near Infrared	30
				Band 5/1.55 -1.75 Shortwave Infrared	30
Landsat 8 OLI/TIRS	31.08.2020	LC08-L2SP-175031	LE07-L1TP-175031	Band 7/ 1.09 -2.35 Shortwave Infrared	30
				Band 1/ 0.43 -0.45 Blue (Coastal Aerosol)	15
				Band 2/ 0.45 -0.51 Blue	30
				Band 3/ 0.53 -0.59 Blue	30
				Band 4/ 0.64 -0.67 Red	30
				Band 5/ 0.85 -0.88 Near Infrared (NIR)	30
				Band 6/ 1.57 -1.65 Shortwave Infrared (SWIR1)	30
Band 7/ 2.11 -2.29 Shortwave Infrared (SWIR2)	30				

Table 3. Source of Additional Data Used as Input Data in Forecasting

Additional data	Source
NDVI	Landsat satellite images
Dem	Aster Dem
Slope	Dem
distancefromriver	Dem

Table 4 Pearson's Correlation with Additional Data

Evaluation	NDVI	Slope	Distance from River	Dem
NDVI		0.09	-0.43	0.63
Slope			-0.09	0.08
DfR				-0.52
Dem				

Table 5. Accuracy Statistics of Classified LU/LC Maps for the Years 2000, 2010 and 2020

Evaluation	2000		2010		2020	
	Pro. accu.	User accu.	Pro. accu.	User accu.	Pro. accu.	User accu.
water	99.46	99.36	99.81	100	99.49	100
Built-up	82.64	98.98	84.57	97.30	95.67	89.33
vegetation	98.45	61.36	99.48	98.92	97.95	99.31
open land	96.43	93.79	99.68	98.89	94.77	95.19
Overall Accuracy	91.28		99.35		97.23	
Kappa Coefficient	0.87		0.99		0.96	

It was mapped by calculating the Euclidean distance from the rivers using the file. After the transition potential matrix was created, the LULC forecast for the year 2020 was modeled. Finally, the LULC simulation of the year 2030 was obtained with the MLP-ANN model. Validation of the model of MLP-ANN is important; therefore, validation between the Q GIS Molusce extension and the MLP-ANN model, the simulated LULC for 2020 and the 2020 LULC, was obtained and the kappa coefficient was obtained.

For the prediction model of 2030, machine learning MLP-ANN algorithm was used in the field of UA and GIS. This model works such as the brain of human, where each neuron node carries information processing between them. nodes which are processing units are interconnected by or ANN with artificial neurons. output a d Input units make up the units processing of the ANN. ANN has a set of learning rules and a result follows. In the training phase of ANN, supervised and unsupervised the methods of learning are performed.

Table 6. 2000-2010 LULC Quantitative Change and Transition Matrix Rates

Class Statistics							
No.	Class name	2000	2010	$\Delta$	2000%	2010%	$\Delta$ %
1	Water	462.16 sq.km.	459.00 sq.km.	-3.16 sq.km.	23.72	23.56	-0.16
2	Built up	159.16	201.37	42.21	8.17	10.33	2.17
3	Vegetation	980.05	655.81	-324.24	50.30	33.66	-16.64
4	Open land	347.19	632.38	285.19	17.82	32.45	14.64
Transition matrix							
	1	2	3	4			
1	0.974559	0.012442	0.012424	0.000574			
2	0.035021	0.373413	0.168249	0.423317			
3	0.00283	0.11201	0.58286	0.3023			
4	0.000731	0.076067	0.149933	0.773269			

Table 7. 2010-2020 LULC Quantitative Change and Transition Matrix Rates

Class Statistics							
No.	Class name	2010	2020	$\Delta$	2010%	2020%	$\Delta$ %
1	Water	459.00 sq.km.	329.56 sq.km.	-129.44 sq.km.	23.56	16.91	-6.64
2	Built up	201.37	300.23	98.87	10.33	15.41	5.07
3	Vegetation	655.81	706.68	50.87	33.66	36.27	2.61
4	Open land	632.38	612.09	-20.30	32.45	31.41	-1.04
Transition matrix							
	1	2	3	4			
1	0.699573	0.295431	0.003802	0.001194			
2	0.006592	0.368937	0.33863	0.285841			
3	0.009902	0.057227	0.726567	0.206305			
4	0.001002	0.083509	0.253423	0.662066			

Table 8: 2000-2020 Land Class Transition Quantitative Data and Matrix Rates 1-Water, 2-Built up, 3-Vegetation, 4-Open land

Cross Class	New Class (2020)	Reference Class (2000)	Pixel Sum	Area (m <sup>2</sup> )	LU-LC Name
1	1	1	356813	321131.7	W
2	1	2	2505	2254.5	BU-W
4	1	3	6314	5682.6	V-W
7	1	4	547	492.3	OL-W
3	2	1	151405	136264.5	W-BU
5	2	2	67909	61118.1	BU
8	2	3	78254	70428.6	V-BU
11	2	4	36026	32423.4	OL-BU
6	3	1	2647	2382.3	W-V
9	3	2	42386	38147.4	BU-V
12	3	3	665914	599322.6	V
14	3	4	74254	66828.6	OL-V
10	4	1	823	740.7	W-OL
13	4	2	82880	74592	BU-OL
15	4	3	321867	289680.3	V-OL
16	4	4	274518	247066.2	OL
Land cover change matrix					
Reference class	New class				
	1	2	3	4	Total
1	32113170	13626450	2382300	740700	460519200
2	2254500	61118100	38147400	74592000	176112000
3	5682600	70428600	59932260	28968030	965114100
4	492300	32423400	66828600	247066200	346810500
Total	32956110	300234600	706680900	612079200	1948555800

Table 9. Quantitative Change in Land Classes between 2020-2030

Class statistics							
	Class cover	2020	2030 (prediction)	2020 %	2030 %	$\Delta$ (2020-2030)	$\Delta$ % (2020-2030)
1	Water	329.56 sq.km.	354.57 sq.km.	16.91%	18.19%	25.01	1.28%
2	Built up	300.23	366.90	15.40	18.82	66.67	3.42
3	Vegetation	706.68	509.09	36.26	26.12	-197.59	-10.14
4	Open land	612.09	718.00	31.41	36.84	105.91	5.43

Table 10. Quantitative Data of LULC Classes Change for All Years

Class statistics					
	Class cover	2000	2010	2020	2030 (prediction)
1	Water	462.16 sq.km.	459.00 sq. km.	329.56 sq. km.	354.57 sq. km.
2	Built up	159.16 sq.km.	201.37 sq. km.	300.23 sq. km.	366.90 sq. km.
3	Vegetation	980.05 sq.km.	655.81 sq. km.	706.68 sq. km.	509.09 sq. km.
4	Open land	347.19 sq.km.	632.38 sq. km.	612.09 sq. km.	718.00 sq. km.
	Class cover	2020%	2030%	$\Delta$ (2020-2030)	$\Delta$ % (2020-2030)
1	Water	16.91%	18.19%	25.01	1.28%
2	Built up	15.40%	18.82%	66.67	3.42%
3	Vegetation	36.26%	26.12%	-197.59	-10.14%
4	Open land	31.41%	36.84%	105.91	5.43%

In the first phase of ANN, data models will be recognized textually and visually. The works of ANN backwards and adjusts the connections network of weight until it produces a minimum of erroneous output (Bose and Chowdhury, 2020; Reddy et al., 2017; Anand and Oinam, 2020).

the model of structure of ANN defined three layers, these layers are the output, hidden and input layers. The ANN of flow working of for datasets of raster is shown in Figure 4. the ANN of the model of each layer consists of neurons which means inputs of user-defined. Representing of the independent and dependent variables are the neurons in the layer of input. The model uses input training examples to obtain classified data in the output layer. In the layer of hidden, the calculations of neurons are made through outputs and weights are produced through the activation function (Islam, Rahman, & Jashimuddin, 2018; e Silva, Xavier, da Silva, & Santos, 2020).

In the prediction model of 2030, LU/LC maps (raster) were used as the basic input data of 2000, 2010 and 2020 (for verification) of the present data. The supplement (auxiliary data) used in the 2030 forecast is shown in the Table 3 below.

Dem is important for geoscientists as it gives quantitative information about the structure of the land (Mukherjee et al., 2013). In the study, altitude map was made by using DEM obtained from Dem data ALOS PALSAR RTC. The high-resolution Alos Palsar Dem data (12.5 m) has been sampled to 30 m in order to have a resolution compatible with the Landsat data to be used in the estimation algorithm.

Calculated based on DEM, this factor shows the slope according to the Literature. It is accepted as one of the factors that have the greatest impact on urbanization (Gao and Li, 2011). In this study, the slope is divided into ten classes. Values were classified between 0 and 197 towards the uphill direction of the slope (Figure 8).

*NDVI Index: Normalized Difference Vegetation Index (Formula 1).*

The NDVI index is the most important data revealing the pressure of urbanization on green areas (Du et al., 2019).

In order to better demonstrate the transformation from green areas in the land cover to built-up areas, the NDVI index was used as the predictive model auxiliary data.

Formula 1. NDVI Index on below

Landsat 7	Landsat 8
B4- B3	B5-B4
B4+B3	B5+B4

Water has been a very important natural resource in the establishment and spread of settlements throughout history. Cities have been established and developed depending on the availability of suitable natural conditions and water resources. In this respect, there is a close relationship between the water resources on earth and the distribution of urban centers. It has been seen that urban areas have been established near fresh water sources such as rivers, lakes and underground waters and on the sea coast for a long time. The horizontal development of cities established near water resources varies depending on the geomorphology and characteristics of the coast and the area behind it (Pektezel, 2015).

By selecting the first and second raster Dem data, a two-way raster comparison was made and all raster data loaded into MOLUSCE was checked. Pearson's correlation was used to compare the data in this study. The correlation coefficient between the data is given in Table 4.

Artificial Neural Network (ANN) machine learning algorithm (Figure 4) was used to model the land use/cover transition potential. The validation sets of the samples and stores the best neural network in memory and the learning algorithm analyzes the accuracy achieved in the training and the best accuracy is reached when the training process ends.

The procedure of validation compares the accuracy of the estimated LULC with the map of LULC obtained by processing Landsat raw data as a reference. The Kappa coefficient was used for validation purposes. It is calculated using the Kappa coefficient, see. Equation 2 (Cohen, 1960).

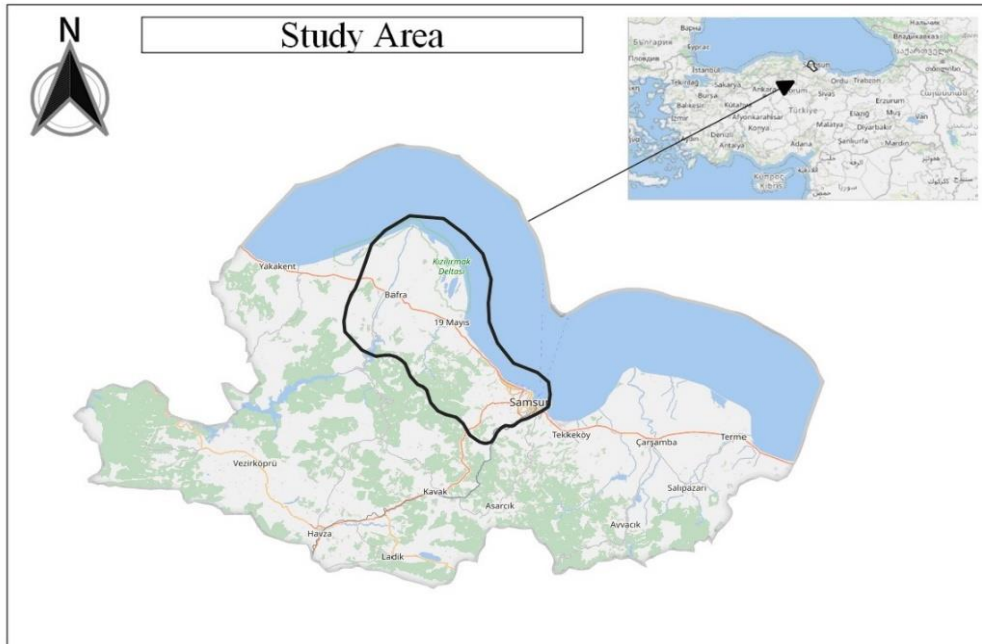


Figure 1. The Study Area

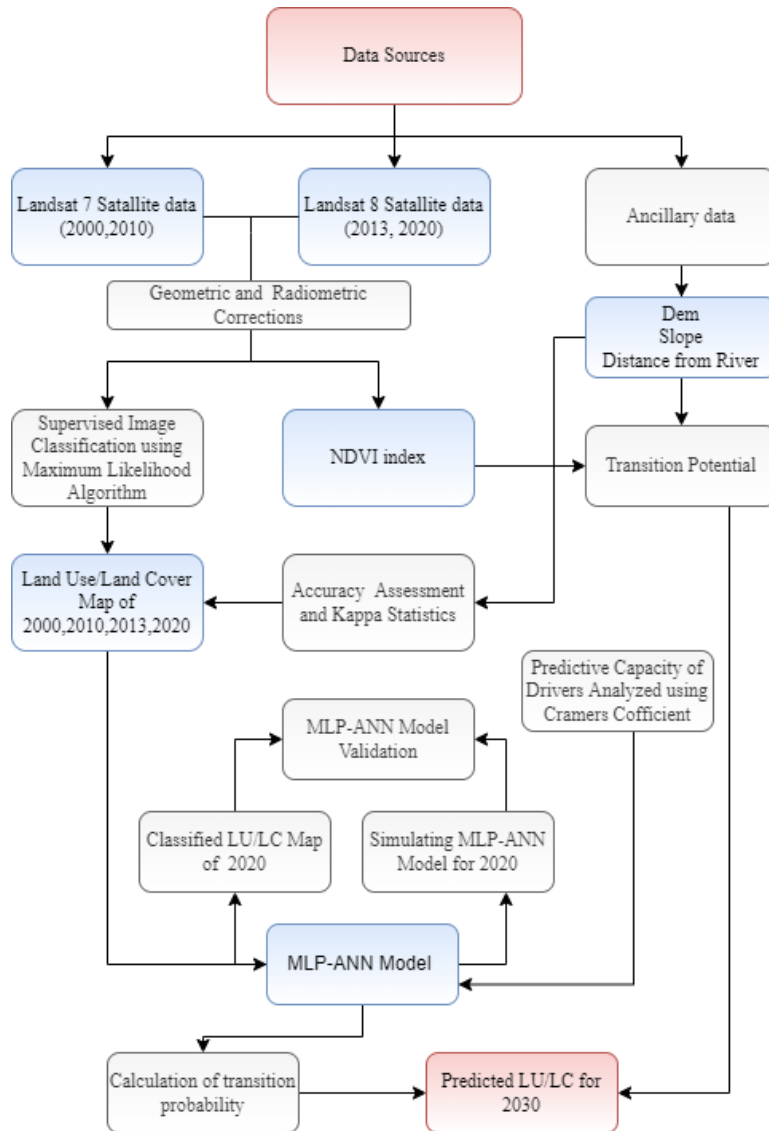


Figure 2 Methodology Flowchart

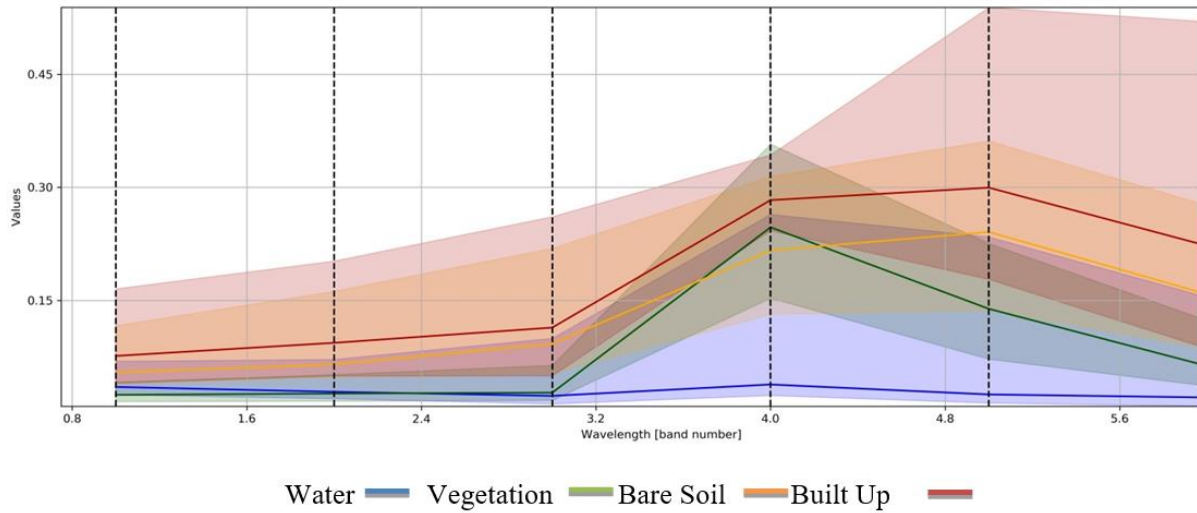


Figure 3. Spectral Signature of Land Classes in LU/LC Map

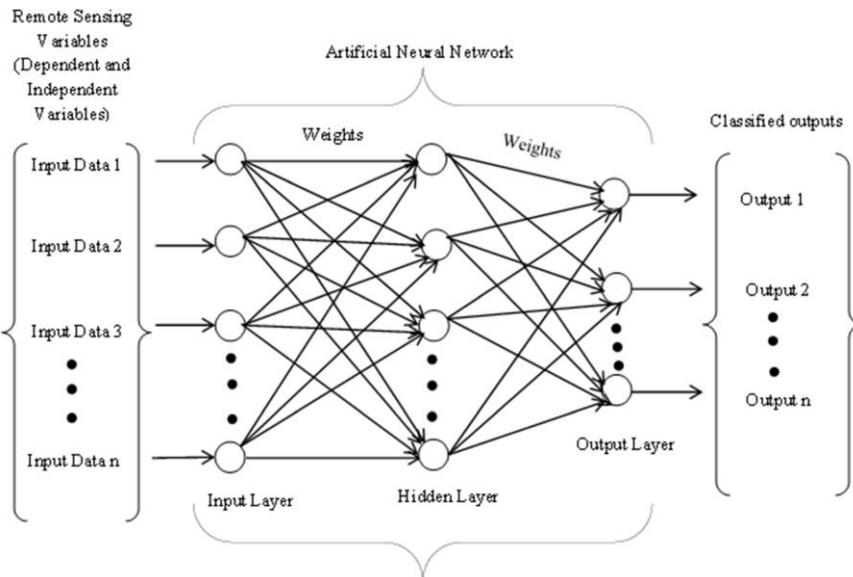


Figure 4. Research steps for Raster Datasets of Neural Network

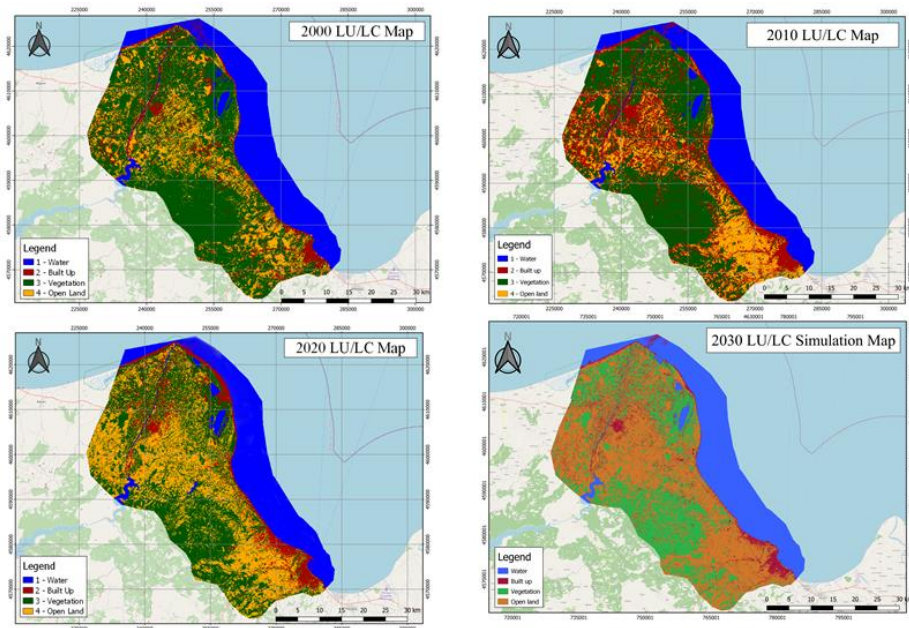


Figure 5. 2000, 2010, 2020, 2030 (Prediction) LULC Maps

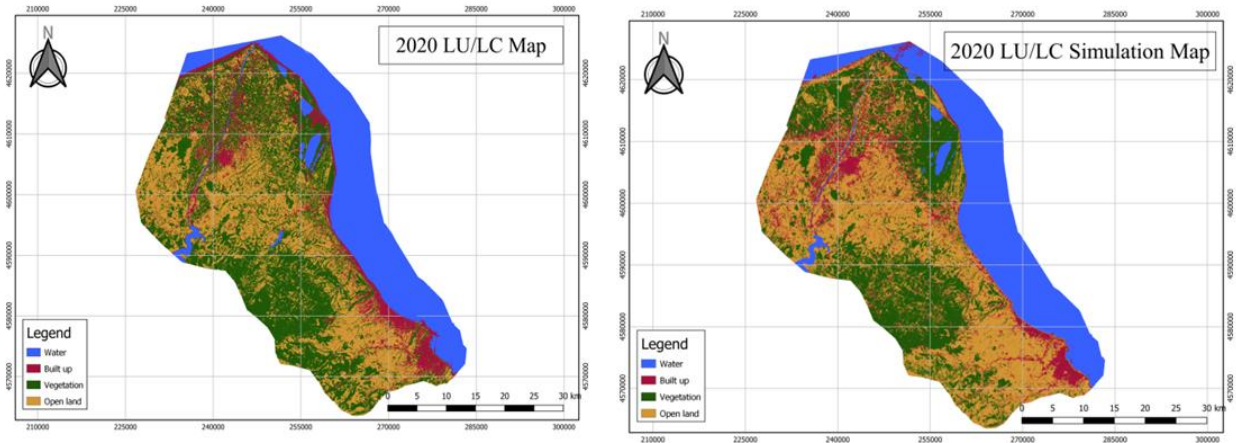


Figure 6 Comparison of (a) 2020 Classified and (b) Forecast Maps

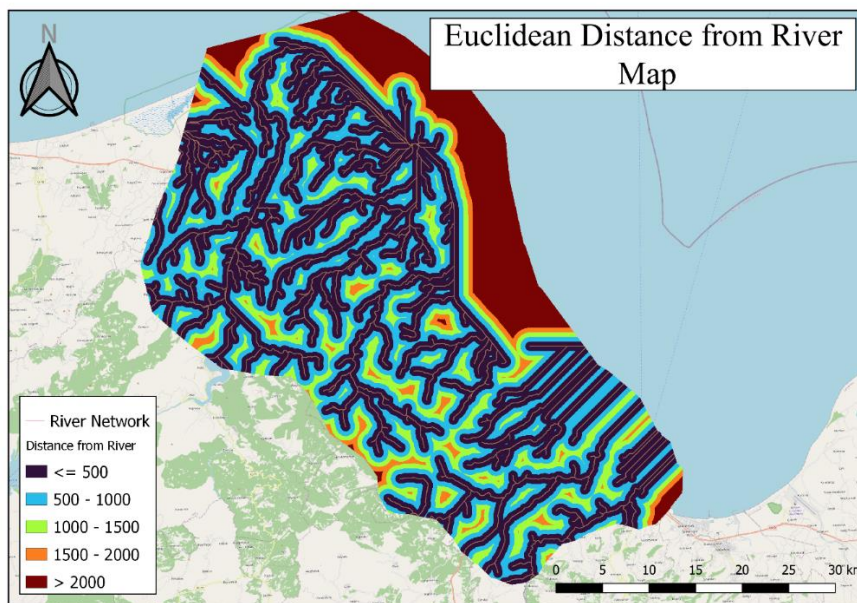


Figure 7 Distance from River Map from Ancillary Data Added to the Forecast Model

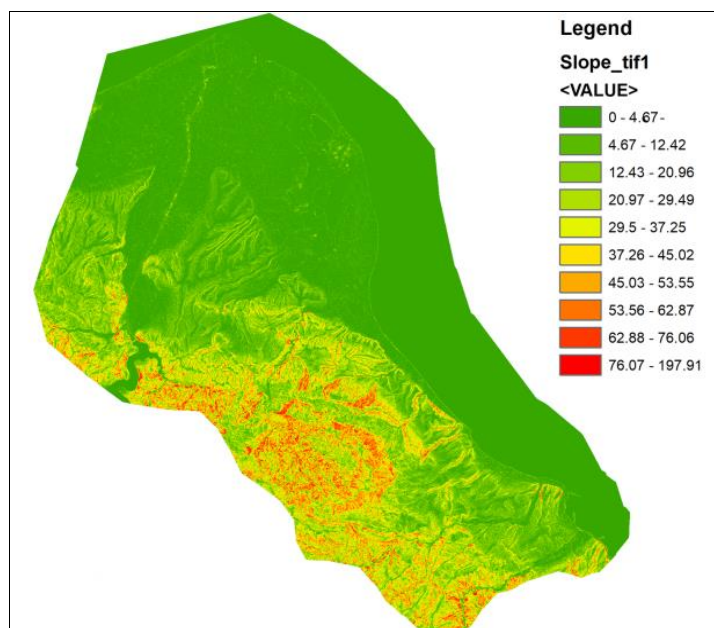


Figure 8 Slope Map from the Auxiliary Data Added to the Forecast Model

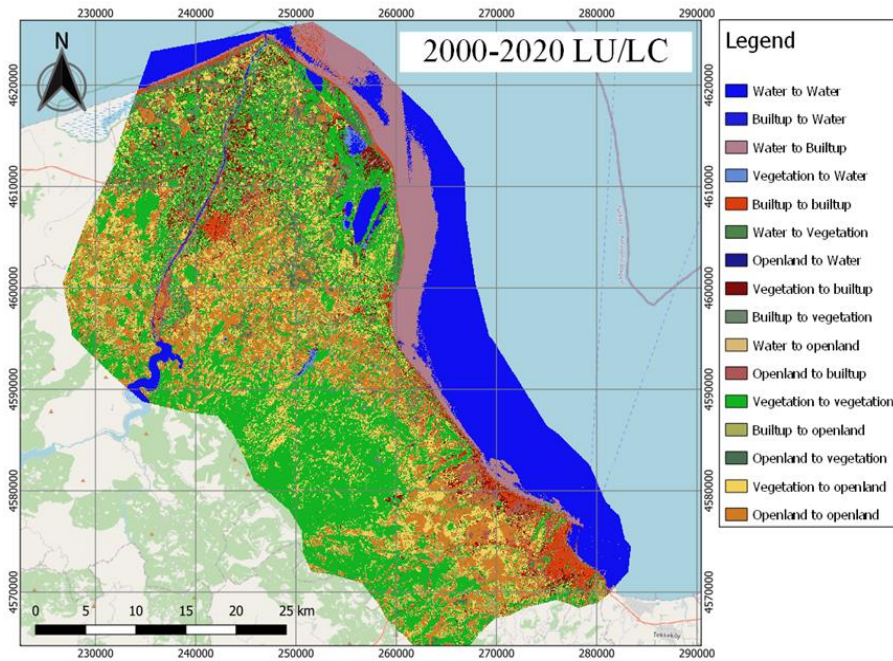


Figure 9. 2000-2020 LU/LC Land Classes Transition Map

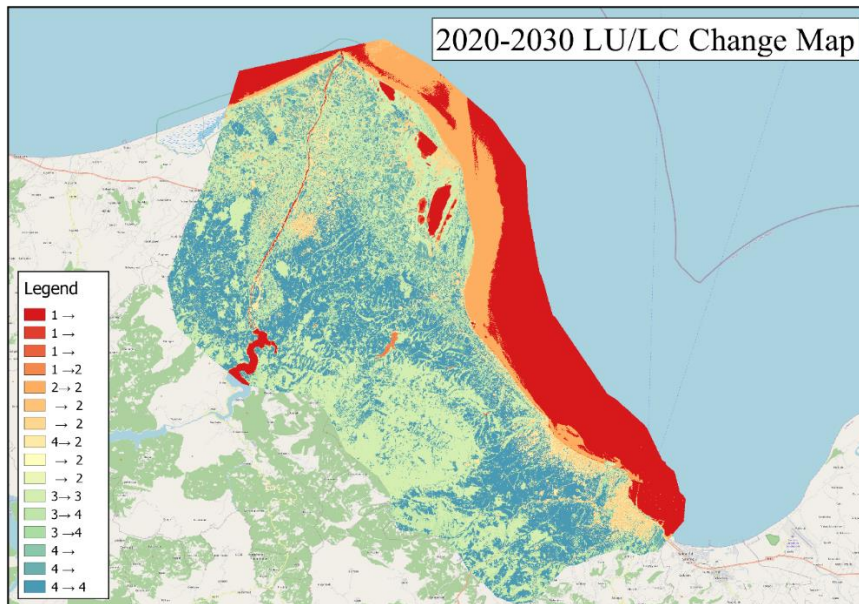


Figure 10. 2020-2030 LU/LC Transition Map between Land Classes 1-Water, 2-Built up, 3-Vegetation, 4-Open land

“I = kappa coefficient;  $x_{ii}$  = value in row and column i,  $x_{i+}$  = sum of row i,  $x_{+i}$  = sum of column i of the matrix, n = total number of observations, and c = total number of classes”. The kappa coefficient classification used is based on (Landis and Koch, 1977), “rating classes: (a) No agreement: < 0, (b) Insignificant agreement: 0.0-0.2 (c) Moderate agreement: 0.2-0.4 (d) Mostly agreement: 0.4-0.6 (e) Significant agreement: 0.6-0.8 and (f) nearly perfect agreement: 0.8-1.0”.

## Results

The changes of LU/LC to better understand, the results are divided into 4 parts: (i.) an accuracy assessment and composition of the LU/LC layers for the years 2000, 2010, 2020; (ii.) change the periods of 2000–2010 analysis; (iii.) 2020 simulation with MLP-ANN method, results of

comparison of simulation with 2020 data of LU/LC, determination of the method that provides the accuracy highest in the research (iv.) land cover forecast for 2030 using the method that gave the best results in the 2020 simulation. The terrain classes maps made using the maximum likelihood algorithm are given in Figure 5.

Parameters of accuracy such as manufacturer and accuracy user, overall accuracy classification and coefficient of kappa of classified the maps of LULC are given in Table 5. overall classification for 2000, 2010, and 2020 of the accuracy classified LULC maps is 91.28%, 99.35%, and 97.23%, respectively. The coefficients of kappa for classified LULC maps are 0.87, 0.99 and 0.96. This indicates that the maps are of satisfactory accuracy to be used for further analysis.

The forecast model of the accuracy of was examined by comparing the 2020 LULC forecast map with the 2020

LULC map classified. The 2020 LULC map was estimated using the 2000 and 2010 LULC maps. The overall accuracy obtained was 72% and the kappa coefficient was 0.65. This shows that the classified and predicted LULC maps of 2020 are in valid agreement with each other. Figure 6 shows that similar inference observed on the basis of visual analysis (). Therefore, it is concluded that the forecast model is capable of simulating the LULC for the year 2030.

After analyzing LU changes between the two periods, relevant co-factors were determined. The co-factors Slope and Distance from River maps obtained from the Dem data are shown in Figure 7 and Figure 8. Pearson Correlation statistic was used to determine the relationship between land use changes and factors. The factors used are given in Table 6.

Each LU/LC category; the first step of the LCM includes rates of change, where land use change trends are evaluated in terms of losses and gains incurred. LULC losses and gains are analyzed for the period 2000-2010, 2010-2020. Tables 6 and 7 give the areas of change in both time periods in km<sup>2</sup> and as percentages. The transition matrix shows the pixel ratios that change from one land use/cover to the next.

Between the years 2000-2010 in Samsun, coastal filling areas were realized especially in Ilkadım district and thus an urban growth was experienced in the northern direction. Batıpark, Doğupark city parks, etc., which were built in the filling area. coastal arrangements, parks and sports fields have been effective in bringing the district to the fore. Filling areas obtained by filling the shores are used as ports, piers, fishermen's shelters, marinas, parks, public institutions and organizations.

The need for housing and social reinforcement areas, which emerged in parallel with the rapid population growth (annual increase rate of 64.5%) in the 2000-2010 period in Atakum district, caused the areal increases in the urban texture to create a more heterogeneous city pattern (Öztürk and Gündüz, 2020). After the 1980s, Atakum has grown in population due to its coastal plains, being far from industrial facilities and the campus of Ondokuz Mayıs University, and it has become an urban development area with the increasing pressure of settlement. It is thought that the increase in urban area in Bafra district is due to the renewal of buildings that have completed their life and secondary housing constructions.

Among the parks on both sides of Samsun, Batıpark is 1.000.000 m<sup>2</sup> and Doğupark is 250.000 m<sup>2</sup>. With the completion of these projects, the green area per capita has reached 9.02 square meters.

Transition Probabilities and Future Projection is an image layer of transition potential represents the probability of transition from one LU/LC class to each another for pixel (Camacho Olmedo, Paegelow, & Mas, 2013). Terrain classified images and ancillary data from the years 2000, 2010, 2020 were used in the prediction model to generate a potential matrix of transition using the QGIS MOLUSCE tool. Molusce used the ANN algorithm to estimate the expected measurable change in LULC classes for the given year using transition potential models. estimated amount of change of LULC of projection of the results in the construction of the transition probability matrix (Ullah et al., 2019). Representing of the matrix is the probability of conversion from one LULC class to

another in 2020 and 2030. cells of diagonal in the transition matrix of probability for 2020 and 2030 reveal the probability of a cell remaining in the class of same LULC between 2 periods.

The variation of LULC classes between land classes over the 2000-2020 time periods is shown in Figure 9 and their quantitative distribution in Table 8. In 2000, the natural green area density in the region can be observed. In 20 years, the water body (River, Lake, Sea) within the determined working area of the region decreased by approximately 7%, the built area (Urban, Roads) increased by 7.24%, green areas (Forest, Cropland, Delta) decreased by 14%, bare It has been determined that areas (Bare Soil) increased by 13.5%.

According to the results obtained, the decrease in the water mass in the study area, which includes Samsun Ilkadım -Atakum - Bafra city centers and the coastline in the 20-year period between 2000 and 2020, shows the transformation into built-up areas by making the shoreline filling area. The decrease in green areas shows the transformation into bare soil areas. With the transformation into bare areas, construction begins. The filling of Samsun coastal areas dates back to the 1960s and accelerates after the 2000s (Karaçuha Yılmaz, 2007). One of the first studies on the construction on the coasts of Samsun (Uzun, 1998) is the research titled "Our Black Sea Coasts in terms of Coastal Law". In this study, it is stated that due to unplanned urbanization, there is a shortage of land that can be allocated to service facilities in the coastal cities of the Black Sea and this problem is tried to be solved with coastal fillings.

The north-eastern part of the region includes the city center. But over the years, it is seen that the settlement has spread in the direction the topography allows. It is seen that the settlement increases in the south-west direction along the coastline. This spread towards rural areas first became a bare area and then transformed into a residential area. The matrix represents that the need for accelerated construction was came primarily by the decline in scrub and soil bare, followed by farmland and sparse vegetation.

According to the results of the algorithm, the ongoing change direction between 2000-2020 is also expected for 2030. The variation of LULC classes between land classes over the time periods 2020-2030 (10 years) is shown in Figure 10 and the quantitative distribution in Table 9. In 10 years, approximately no change is observed in the water body (River, Lake, Sea) within the determined working area boundary of the region, built up area (Urban, Roads) increased by 3.42%, green areas (Forest, Cropland, Delta) decreased by 10.14%, bare areas (Bare Soil) It is estimated that there will be an increase of 5.43%. It is estimated that the decrease in the water body in the study area will end in this last 10 years. This can be interpreted as the saturation of Samsun coastal areas with area gain by filling. It is estimated that there will be a transformation from green areas to bare areas first, and then there will be a conversion to build areas. The 10% decrease in green areas is shared between bare areas and green areas in the direction of increase. Considering the spectral signatures of the Land Types, the signatures of bare areas and built areas are very close to each other. For this reason, the rate of segregation between bare areas and built areas is not sensitive. It is expected that the spread of the city centers along the river

in the rural district and along the sea coast in the central districts and in the south-west direction in accordance with the topographic structure will continue in this 10-year period. Looking at the land classes transition map in Figure 10, it is seen that the direction of change seen in previous years continues in 2030. Green areas, especially in rural areas, are transformed into bare areas, and from bare areas to build areas.

## Discussions

Due to the environmental problems caused by rapid and uncontrolled urbanization, studies to understand the land change and to predict possible changes in the future are increasing rapidly. datasets of remote sensing, available as open access, economical, up-to-date, and archival, are the most common systems used for spatial/temporal modeling and to determine LU/LC changes and urban growth. In this study, the LULC change between 2000, 2010, 2020 for the study area including İlkadım, the central district where the development is most intense in Samsun, the largest port city of the Black Sea, Atakum along the coastline, and Bafra, the rural district with the most agricultural lands, were analyzed and a land change forecast for 2030 was made using the MLP-ANN (multi-layer perception artificial neural network) algorithm. The rate of land change for the years 2000, 2010, 2020, 2030 is shown in Table 10.

For the accuracy of the study, precautions were taken during the data download and processing stages. For example, we preferred satellite images of the summer months and recent dates so that the land cover can be seen more clearly due to seasonal factors. During the download phase of the satellite images, we determined the cloud-free rate, and at the same time, we separated the cloud-free images during the preview phase of the images. In the land classification stage, since the spectral signatures of bare soil and built areas are similar to each other, the two classes are mixed. We re-checked this separation with the Jeffries-Matusita distance meter and repeated the samples with close values. However, there are many different factors that will affect the accuracy in estimation studies. For example, heterogeneity of land in urban areas affects the results. Due to technical errors, situations that may affect the accuracy of the model may occur at the classification stage. In addition, factors of human activities are not taken into account in the estimation of LULC data (Lu, Wu, Ma, & Li, 2019). It is not possible to provide this data for previous years. When we added the road network data to the model, we saw that the accuracy decreased. Therefore, a stream network has been added instead of this data. However, if sufficient and accurate data on policy, socioeconomic, demographics, road network and come in the future, it is advised to integrate into the model of MLP-ANN the data.

Ozturk, (2015) chose Samsun Atakum district as the study area and compared the kappa accuracy coefficients of the results of the two estimation algorithms (CA-MC and MLP-MC) and stated that the most accurate method was MLP-MC Multi-Layer Perceptron-Markov Chain. can reach figures that will be considered valid and useful for all algorithms, but the preference of machine learning (ANN) in this study has added up-to-dateness to the study. As a result of the study and in the literature review, it is seen that

the auxiliary data added to the estimation algorithm are important data that affect the land change, their numbers and accuracy affect the accuracy coefficient of the algorithm. For example, Hakim, Baja, Rampisela, and Arif, (2021) provided 0.89% accuracy by using ten auxiliary data in their study. These data are Population density per pixel, Distance from road, Distance from education facility, Elevation, Distance from health facility, Distance from sea, Distance from CBD, Distance from downtown, Slope, Distance from river.

Hamad, Balzter, and Kolo (2018) achieved an accuracy rate of 80% based on two scenarios. In addition, the prediction trends of LULC classes should be evaluated with increasing environmental involvement. Ullah et al., (2019) simulated LULC changes for the period 2032 and 2047 using the transition potential matrix from the data of 2002 and 2017. A cellular automaton and artificial neural network (CA-ANN) prediction model was used. Distance and height auxiliary data from major roads were used. Thus, it is seen that the selection of auxiliary data plays an important role in the accuracy rate of the prediction algorithm.

## Conclusions

Remote sensing methods are one of the most efficient methods used to analyze spatial and temporal terrain change. Machine learning for prediction is one of the methods that has emerged in recent years. In the current study, it was deemed appropriate to use the artificial neural network (MLP-ANN) algorithm. Considering the results, the conversion of fertile lands to bare land and built lands will create future ecological problems and unproductive areas that cannot meet the natural food requirement.

Our study does not currently include estimates of the impact of land change on climate change, but as Albers et al., (2015) stated in his study, it is important to control land use change, especially in the context of global climate change. As a result of irregular urbanization, climate change and global warming will be inevitable. It is necessary to find more effective solutions to reduce this negative effect without wasting more time and green space. This study will guide the decision makers in the planning phase, which will help in the field of natural resources management.

## Suggestions

Based on the results, ongoing planning criteria need to be reconsidered to prevent loss of farmland and other vegetation. It is strongly recommended that the population spread should be shaped according to the new plans. In the planning phase, multidisciplinary teams consisting of city planners, landscape architects, surveyors and architects should be formed and joint work should be done. Urbanization plans cannot be considered by ignoring the ecological characteristics and habitat of the area.

## Acknowledgements

As authors, I would like to thank my Ph.D. advisor of Kastamonu University and her advisory is Assoc. Prof. Dr. Mehmet Cetin for their support and assistance. This research

has been produced from a part of Burcu Çevik Değerli's Ph.D. dissertation in Kastamonu University, Institute of Science, and Department of Landscape Architecture.

## References

- Aburas MM, Ahamad MSS, Omar NQ. 2019. Spatio-temporal simulation and prediction of land-use change using conventional and machine learning models: a review. *Environmental monitoring and assessment*, 191(4): 1-28.
- Alqadhi S, Mallick J, Balha A, Bindajam A, Singh CK, Hoa PV. 2021. Spatial and decadal prediction of land use/land cover using multi-layer perceptron-neural network (MLP-NN) algorithm for a semi-arid region of Asir, Saudi Arabia. *Earth Science Informatics*, 14(3): 1547-1562.
- Anand V, Oinam B. 2020. Future land use land cover prediction with special emphasis on urbanization and wetlands. *Remote Sensing Letters*, 11(3): 225-234.
- Anonim a. (Date of access: 05.06.2021). Provincial and District Areas. Retrieved from <https://harita.gov.tr/urun/il-ve-ilce-yuzolcumleri/176>.
- Anonim b. (Date of access: 06.06.2021). Samsun Integrated Coastal Areas Management and Planning Project-Spatial Strategy Plan, 208p.
- Anonim c. (Date of access: 02.05.2021). Statistical indicators. Retrieved from <https://data.tuik.gov.tr/Bulten/Index?p=Adrese-Dayali-Nufus-Kayit-Sistemi-Sonuclari-2020-37210>.
- Bağcı H, Bahadır M. 2019. Land Use and Temporal Change in the Kızılırmak Delta (Samsun) (1987-2019). *The Journal of Academic Social Science Studies*, 34: 295-312.
- Municipality A. 2014). 2015-2019 STRATEGIC PLAN.
- Municipality SB. (Date of access: 27.01.2022). 2020 – 2024 Strategic Plan. Retrieved from <https://www.samsun.bel.tr/>
- Benediktsson JA, Swain PH, Ersoy OK. 1990. Neural network approaches versus statistical methods in classification of multisource remote sensing data. Vancouver, Canada, July 10-14, 1989) *IEEE Transactions on Geoscience and Remote Sensing*.
- Blanco-Canqui H, Lal R. 2008. *Principles of soil conservation and management*: Springer Science & Business Media.
- Bose A, Chowdhury IR. 2020. Monitoring and modeling of spatio-temporal urban expansion and land-use/land-cover change using markov chain model: a case study in Siliguri Metropolitan area, West Bengal, India. *Modeling Earth Systems and Environment*, 6(4): 2235-2249.
- Bounouh O, Essid H, Farah IR. 2017. Prediction of land use/land cover change methods: A study. Paper presented at the 2017 international conference on advanced technologies for signal and image processing (ATSIP).
- Camacho Olmedo M, Paegelow M, Mas JF. 2013. Interest in intermediate soft-classified maps in land change model validation: suitability versus transition potential. *International Journal of Geographical Information Science*, 27(12): 2343-2361.
- Cohen J. 1960. A coefficient of agreement for nominal scales. *Educational and psychological measurement*, 20(1): 37-46.
- Congedo L. 2016. Semi-automatic classification plugin documentation. Release, 4(0.1): 29.
- Congedo L. 2021. Semi-Automatic Classification Plugin: A Python tool for the download and processing of remote sensing images in QGIS. *Journal of Open-Source Software*, 6(64): 3172.
- Du J, Fu Q, Fang S, Wu J, He P, Quan Z. 2019. Effects of rapid urbanization on vegetation cover in the metropolises of China over the last four decades. *Ecological Indicators*, 107: 105458.
- E Silva LP, Xavie, APC, Da Silva RM, Santos CAG. 2020. Modeling land cover change based on an artificial neural network for a semiarid river basin in northeastern Brazil. *Global Ecology and Conservation*, 21: e00811.
- Fernando HJS, Dimitrova R, Sentic S. 2012. Climate change meets urban environment. In *National Security and Human Health Implications of Climate Change* (pp. 115-133): Springer.
- Gao J, Li S. 2011. Detecting spatially non-stationery and scale-dependent relationships between urban landscape fragmentation and related factors using Geographically Weighted Regression. *Applied Geography*, 31(1): 292-302.
- Güler M, Yomralıoğlu T, Reis S. 2007. Using landsat data to determine land use/land cover changes in Samsun, Turkey. *Environmental monitoring and assessment*, 127(1): 155-167.
- Hakim AMY, Baja S, Rampisela DA, Arif, S. 2021. Modelling land use/land cover changes prediction using multi-layer perceptron neural network (MLPNN): a case study in Makassar City, Indonesia. *International Journal of Environmental Studies*, 78(2): 301-318.
- Hamad R, Balzter H, Kolo K. 2018. Predicting land use/land cover changes using a CA-Markov model under two different scenarios. *Sustainability*, 10(10): 3421.
- Islam K, Rahman MF, Jashimuddin M. 2018. Modeling land use change using cellular automata and artificial neural network: the case of Chunati Wildlife Sanctuary, Bangladesh. *Ecological Indicators*, 88: 439-453.
- Jamali A. 2019. A fit-for-purpose algorithm for environmental monitoring based on maximum likelihood, support vector machine and random forest. *Int Arch Photogramm Remote Sens Spatial Inf Sci*, 42(3/W7): 25-32.
- Jensen JR. 1986. *Introductory digital image processing: a remote sensing perspective*. Retrieved from
- Karaçuha Yılmaz E. 2007. Examination of the Coastal Fill Area of Samsun City in terms of Landscape Architecture and Suggestions. In: Ankara University, Department of Landscape Architecture, Master Thesis
- District Government A. 2013. *While Changing, Developing Atakum*.
- Landis R, Koch GG. 1977. An application of hierarchical kappa-type statistics in the assessment of majority agreement among multiple observers. *Biometrics*, 363-374.
- Lee SY, Song XY. 2004. Evaluation of the Bayesian and maximum likelihood approaches in analyzing structural equation models with small sample sizes. *Multivariate Behavioral Research*, 39(4): 653-686.
- Lu Y, Wu P, Ma X, Li X. 2019. Detection and prediction of land use/land cover change using spatiotemporal data fusion and the Cellular Automata–Markov model. *Environmental monitoring and assessment*, 191(2): 1-19.
- MohanRajan SN, Loganathan A. 2021. Modelling spatial drivers for LU/LC change prediction using hybrid machine learning methods in Javadi Hills, Tamil Nadu, India. *Journal of the Indian Society of Remote Sensing*, 49(4): 913-934.
- MohanRaja SN, Loganathan A, Manoharan P. 2020. Survey on Land Use/Land Cover (LU/LC) change analysis in remote sensing and GIS environment: Techniques and Challenges. *Environmental Science and Pollution Research*, 27(24): 29900-29926.
- Mukherjee S, Joshi PK, Mukherjee S, Ghosh A, Garg R, Mukhopadhyay A. 2013. Evaluation of vertical accuracy of open-source Digital Elevation Model (DEM). *International Journal of Applied Earth Observation and Geoinformation*, 21: 205-217.
- Ozturk D. 2015. Urban growth simulation of Atakum (Samsun, Turkey) using cellular automata-Markov chain and multi-layer perceptron-Markov chain models. *Remote Sensing*, 7(5): 5918-5950.
- Ozturk D. 2017. Assessment of urban sprawl using Shannon's entropy and fractal analysis: a case study of Atakum, Ilkadam and Canik (Samsun, Turkey). *Journal of environmental engineering and landscape management*, 25(3): 264-276.
- Öztürk D, Gündüz U. 2020. Determination of Temporal Changes in Urban Tissue Morphology in Samsun Districts by Fractal Analysis. *Dokuz Eylül University Faculty of Engineering Journal of Science and Engineering*, 22(64): 81-95.

- Paola JD, Schowengerdt RA. 1995. A review and analysis of backpropagation neural networks for classification of remotely-sensed multi-spectral imagery. *International Journal of Remote Sensing*, 16(16): 3033-3058.
- Pektezel H. 2015. City and Water Resources. In (pp. 107-132).
- Reddy CS, Singh S, Dadhwal V, Jha C, Rao NR, Diwakar P. 2017. Predictive modelling of the spatial pattern of past and future forest cover changes in India. *Journal of Earth System Science*, 126(1): 1-16.
- Saleem A, Corner R, Awange J. 2018. On the possibility of using CORONA and Landsat data for evaluating and mapping long-term LULC: Case study of Iraqi Kurdistan. *Applied Geography*, 90: 145-154.
- Sesli FA. 2010. Mapping and monitoring temporal changes for coastline and coastal area by using aerial data images and digital photogrammetry: A case study from Samsun, Turkey. *International Journal of Physical Sciences*, 5(10): 1567-1575.
- Turner BL, Skole D, Sanderson S, Fischer G, Fresco L, Leemans R. 1995. Land-use and land-cover change: science/research plan. *Global Change Report (Sweden)*, 43: 669-679.
- Ullah S, Tahir AA, Akbar TA, Hassan QK, Dewan A, Khan AJ. 2019. Remote sensing-based quantification of the relationships between land use land cover changes and surface temperature over the Lower Himalayan Region. *Sustainability*, 11(19): 5492.
- University Y. 2020. (Erişim tarihi: 01.08.2020). Center for Earth Observation, Landsat. Retrieved from <https://yceo.yale.edu/how-convert-landsat-dns-albedo>,
- USGS. 2020. (Erişim tarihi: 09.04.2020). Landsat Missions. Retrieved from <https://www.usgs.gov/land-resources/nli/landsat>
- Uzun A. 1998. Our Black Sea coasts in terms of coastal law. *Jeomorfoloji Dergisi*, 21: 60-64.
- Wu J. 2014. Urban ecology and sustainability: The state-of-the-science and future directions. *Landscape and urban planning*, 125: 209-221.
- Yao Z, Wang B, Huang J, Zhang Y, Yang J, Deng R. 2021. Analysis of Land Use Changes and Driving Forces in the Yanhe River Basin from 1980 to 2015. *Journal of Sensors*, 2021.
- Yirsaw E, Wu W, Shi X, Temesgen H, Bekele B. 2017. Land use/land cover change modeling and the prediction of subsequent changes in ecosystem service values in a coastal area of China, the Su-Xi-Chang Region. *Sustainability*, 9(7): 1204.
- Zhou W, Pickett ST, Cadenasso ML. 2017. Shifting concepts of urban spatial heterogeneity and their implications for sustainability. *Landscape ecology*, 32(1): 15-30.